International Journal of Rock Mechanics & Mining Sciences 153 (2022) 105107

Contents lists available at ScienceDirect

International Journal of Rock Mechanics and Mining Sciences

journal homepage: www.elsevier.com/locate/ijrmms

Modelling anisotropic adsorption-induced coal swelling and stress-dependent anisotropic permeability

Min Chen *, Shakil Masum, Sivachidambaram Sadasivam, Hywel Thomas

Geoenvironmental Research Centre, Cardiff School of Engineering, Cardiff University, CF24 3AA, Cardiff, United Kingdom

ARTICLE INFO

Keywords:
Modelling
Effective stress
Anisotropy
Coal swelling
Coal permeability

ABSTRACT

To investigate the anisotropy of coal swelling, this study proposes an effective stress model for saturated, adsorptive fractured porous media by considering gas adsorption induced surface stress change on solid-fluid interface. The effective stress model can be used to capture the anisotropic swelling of coal combining anisotropic mechanical properties and to link with the anisotropic permeability. Direction dependent fracture compressibility is used to describe the evolution of anisotropic stress-dependent permeability behaviour. Particularly, the impact of gas adsorption on fracture compressibility is considered in the model. The proposed models were tested against experimental results and compared to relevant existing models available in literatures. The model predicts that the coal swelling in the direction perpendicular to the bedding plane, is greater than that in the parallel plane. Coal permeability in each direction can be affected by the stress changes in any directions. The permeability parallel to the bedding plane is more sensitive to change in stresses than in perpendicular to the bedding due to higher fracture compressibility. The cleat compressibility could increase with gas adsorption, especially for carbon dioxide. Permeability loss in the direction parallel to the bedding plane is more significant than that in the direction perpendicular to the bedding plane. The presented models provide a tool for quantifying gas adsorption-induced anisotropic coal swelling and permeability behaviours.

1. Introduction

Coalbeds are often recognised as energy resources and storage reservoirs for geological sequestration of greenhouse gases, such as, carbon dioxide (CO_2). Due to its extensive volume, the global coal deposits have significant potential to reduce the emission of CO_2 into the atmosphere.[1] Over the years, a number of field demonstration projects have been conducted across the world to store CO_2 in coal seams.[2,3] The pilot trials regularly reported the swelling-induced loss of gas injectivity and struggled to achieve a sustained rate of gas injection into the seams.[4–7] CO_2 adsorption in coal results in swelling of the coal matrix and reduce the permeability at the vicinity of the injection well.[8,9] This leaves the bulk of the coal seam unused and questions the feasibility and practicality of the technologies pertinent to carbon sequestration in coal. Therefore, to address the gas injection and storage issues, comprehensive understanding of coal swelling and permeability behaviours are of paramount importance.

Coalbeds are naturally fractured sedimentary rocks, and are generally characterised by i) a well-defined and nearly uniform distributed network of natural fractures, known as cleats, and ii) by multiscale porous blocks that reside between the fractures, known as coal matrix.[10] Coal contains two distinct types of cleats, e.g., face cleat and butt cleat. The face cleats are well-developed, widely spaced, nearly parallel fissures that run continuously throughout a coal seam. Butt cleats are perpendicular to the face cleats and poorly-developed fractures of limited length, and often terminate at the face cleats. Both type of cleats are nominally vertical, and perpendicular to the bedding planes.[11,12] Cleat system provides the primary conduits for fluid flow in coalbeds,[12] and the permeability of coal is predominantly dependent on the properties of the cleat networks. The distribution of cleats in coalbeds leads to anisotropic permeability where the greatest permeability occurs in the direction of the face cleats. This has been observed in both field observations and laboratory measurements and, therefore, questions the notion of isotropic material behaviour that is often considered in theoretical and numerical modelling studies. For example, Koenig and Stubbs[13] reported that from the field tests in the Rock Creek coalbeds of the Warrior Basin in the USA, the permeability of coal in the direction parallel to the bedding plane is 17 times higher than that of the direction

* Corresponding author.
E-mail address: Chenm24@cardiff.ac.uk (M. Chen).

https://doi.org/10.1016/j.ijrmms.2022.105107
Received 1 May 2021; Received in revised form 17 November 2021; Accepted 22 March 2022
Available online 2 April 2022

vertical to the bedding plane. Massarotto et al.[14] investigated the permeability anisotropy of coals using a unique true tri-axial test in laboratory coal samples, and they reported that the permeability of coal was significantly directional. Another important, anisotropic property of coal is the directional swelling. Many laboratory experiments have confirmed the anisotropy of coal swelling. Day et al.[15] measured the CO_2 adsorption-induced swelling of three Australian bituminous coals at pressures up to 15 MPa with an optical method, and observed that the swelling in the plane perpendicular to the bedding plane was always significantly higher than that of the parallel plane. Similar results have been reported by Pan and Connell[16] and Liu et al.[17] The consequence of adsorption-induced coal deformations is that the in-situ stress field becomes disturbed,[7] and it can further change the permeability behaviour. Therefore, accurate representation of the anisotropic coal swelling together with anisotropic permeability is essential.

Permeability change in coal is generally attributed to the net impacts of both effective stress and adsorption/desorption induced swelling/shrinkage stress or strains.[9] Based on this concept, many permeability models have been developed to study the permeability behaviour of coals. A comprehensive review of these models is available in Liu et al.[18] and Pan and Connell.[9] Majority of these models assumed isotropy of coal properties and swelling behaviour. The permeability evolution is generally linked to the change in coal porosity using a cubic relationship between permeability, porosity, and different stress–strain relationships. Undoubtedly, these previous studies have enriched our understanding of coal permeability evolution, nevertheless, the anisotropy of the material and its behaviour have been often neglected. Gu and Chalaturnyk[19] suggested that the change of permeability is anisotropic (due to the difference between butt cleats and face cleats) even though the initial permeability is assumed to be isotropic. The results presented by Liu et al.[20] indicated that the application of isotropic deformation in permeability model could overestimate the permeability loss compared to the anisotropic deformation. Thus, anisotropic deformation should be considered to predict the coal permeability behaviour.

In recent years, a few anisotropic permeability models have been proposed to study the directional permeability behaviour of coal. Wang et al.[21] developed an anisotropic permeability model by incorporating anisotropy of structural and mechanical deformation. Liu et al.[22] derived a cleat aperture-dependent anisotropic permeability model, in which, a modulus reduction ratio is used to link the anisotropic deformation to the evolution of directional permeabilities. Pan and Connell[16] presented an anisotropic permeability model by extending the swelling model of Pan and Connell.[23] Like most of the isotropic permeability models, the aforementioned models assumed that the impacts of effective stress and shrinkage/swelling on coal permeability are independent. Pure stress or strain superposition was used to obtain the total changes in stress or strain, which was resulted from the pressure change and the shrinkage/swelling of the coal matrix. Actually, changes of strain or stress caused by pressure and shrinkage/swelling of coal are inter-related, especially under in situ conditions.[24] The coupled anisotropic permeability model developed by Gu and Chalaturnyk[19] shows some advantages in the analysis of anisotropic permeability, which considers discontinuous coal mass (containing cleats and matrix) to be an equivalent elastic continuum taking into account the cleat structure and characteristics of cleat deformation. However, the aperture changes in different directions are still quantified with the principle of strain superposition. The deformation of cleat aperture is closely related to cleat compressibility.[25] Recent studies show that coal-gas interaction can alter the cleat compressibility,[26] this important coupled effect has been ignored in the previous permeability models.

The purpose of this work is to present a comprehensive model that accounts for both anisotropic swelling and permeability behaviour in a practical and rigorous manner. Adsorption of gases on pores of coal matrices can alter the surfaces stress, influencing its effective stress. Firstly, an effective stress model for an anisotropic fractured porous media with dual porosity is derived using the surface stress approach. It is then used to describe anisotropic macroscopic coal swelling with anisotropic mechanical properties. Compared to the exiting anisotropic swelling model, the number of required parameters is reduced in the proposed model. An anisotropic, stress-dependent coal permeability model is then derived, in which directional fracture compressibilities are introduced. Stress or strain superposition is avoided compered to existing permeability models. More importantly, the impact of coal-gas interaction on cleat compressibility is considered in the proposed model. These new features of model could advance the understandings of coal permeability evolution. The accuracy and reliability of the developed models are examined by comparing the model results with relevant experimental data. Finally, the impacts of anisotropic swelling on coal permeability are investigated for different boundary conditions. The model can be used to study the mechanisms that control deformation and anisotropic permeability evolutions of coal, which are important for better predictions and analysis of subsurface carbon sequestration and coalbed methane recovery techniques.

2. The model

2.1. Theoretical development of anisotropic deformation

Assuming that the deformation behaviour of a fractured coal is linear and elastic, the stress-strain relationship can be expressed in an incremental form as:[27]

$$d\sigma'_{eij} = C_{ijkl} d\varepsilon_{kl} \tag{1}$$

or

$$d\varepsilon_{ij} = D_{ijkl} d\sigma'_{ekl} \tag{2}$$

where σ'_{eij} or σ'_{ekl} is a component of second-order stress tensor, ε_{ij} or ε_{kl} is a component of second-order strain tensor. C_{ijkl} and D_{ijkl} are respectively fourth order elastic stiffness and elastic compliance tensors, and $\boldsymbol{D} = \boldsymbol{C}^{-1}$.

Considering a multi-phase system that includes solid aggregates, bulk fluids in fractures and in porous matrix, as well as adsorbed fluids at the interface between the solid and the bulk fluid (see Fig. 1), the effective stress (σ'_{eij}) for the bulk coals can be expressed as (see Appendix for the detailed derivation):

$$\sigma'_{eij} = \sigma_{ij} + p_f^s \delta_{ij} + b_{mij}\left(p_m - p_m^s\right) + b_{fij}\left(p_f - p_f^s\right) \tag{3}$$

where σ_{ij} is the total stress, p_m is fluid pressure in matrix pores, p_f is fluid pressure in fracturs. b_{mij} and b_{fij} are effective stress coefficients associated with fluid pressures in matrices and fractures, respectively. Adsorption of gases in coal alters its surface stresses. The effect is calculated using p_m^s and p_f^s as:

$$p_m^s = \xi_m \sigma^s \tag{4}$$

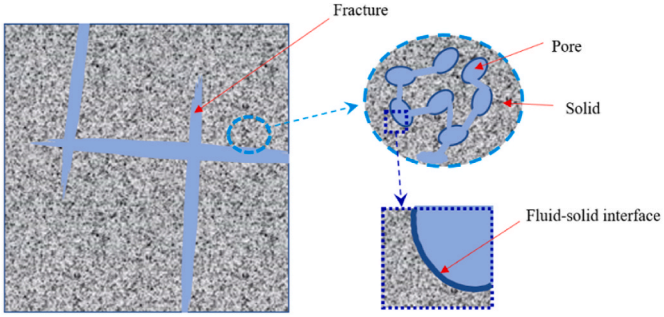

Fig. 1. Schematics of a fractured porous media saturated with fluids.

$$p_f^s = \xi_f \sigma^s \tag{5}$$

where ξ_f and ξ_m are material parameter constants representing the correlations between the adsorption surface area and the volumetric strain and porosity (see Appendix).

Based on the Gibbs' law, Nikoosokhan et al.[28] described the change in surface stress at the fluid-solid interface as:

$$\Delta\sigma^s = -\int_{p_{m0}}^{p_m} \Gamma \overline{V}_b dp_m \tag{6}$$

where p_{m0} is the pressure at reference state, Γ is the number of moles of fluid molecules adsorbed per unit area of the fluid-solid interface, and $\overline{V}_b = RT/p_m$ is the molar volume of the bulk fluid. Given that the fluid adsorption obeys Langmuir isotherm:[3]

$$\Gamma = \frac{\Gamma^{max} b_L p_m}{p_m b_L + 1} \tag{7}$$

where Γ^{max} is the Langmuir adsorption constant, representing the adsorption capacity of fluid per unit adsorption surface, and b_L is the Langmuir pressure constant. By considering the adsorption isotherm, the change in surface stress for a gas mixture, is expressed as:[29]

$$\Delta\sigma^s = -\frac{RT\sum_{m=1}^{n_g} \Gamma_m^{max} b_{Lm} x_m}{\sum_{m=1}^{n_g} b_{Lm} x_m} \ln\left(1 + p_m \sum_{m=1}^{n_g} b_{Lm} x_m\right) \tag{8}$$

where x_m is the molar fraction of the mth gas component, R is universal gas constant, T is temperature, and n_g is the number of gas components in the mixture.

The fourth order D_{ijkl} tensor in equation (2) has 81 components. Considering that coal behaves as an orthotropic, elastic material,[30] and employing Betti-Maxwell reciprocal relation $D_{ijkl} = D_{klij}$, as well as the symmetry of the stress and strain tensors, the constitutive equations of an orthotropic material can be expressed as[27]:

$$\begin{bmatrix} \varepsilon_{11} \\ \varepsilon_{22} \\ \varepsilon_{33} \\ \varepsilon_{12} \\ \varepsilon_{13} \\ \varepsilon_{23} \end{bmatrix} = \begin{bmatrix} d_{11} & d_{12} & d_{13} & 0 & 0 & 0 \\ d_{12} & d_{22} & d_{23} & 0 & 0 & 0 \\ d_{13} & d_{23} & d_{33} & 0 & 0 & 0 \\ 0 & 0 & 0 & d_{44} & 0 & 0 \\ 0 & 0 & 0 & 0 & d_{55} & 0 \\ 0 & 0 & 0 & 0 & 0 & d_{66} \end{bmatrix} \begin{bmatrix} \sigma'_{e11} \\ \sigma'_{e22} \\ \sigma'_{e33} \\ \sigma'_{e12} \\ \sigma'_{e13} \\ \sigma'_{e23} \end{bmatrix} \tag{9}$$

where d is the compliance coefficient. It can be seen from equation (9) that only nine nonzero stiffness are independent for orthotropic materials. By introducing the elastic parameters, equation (9) is rewritten as:[31]

$$\begin{bmatrix} \varepsilon_{xx} \\ \varepsilon_{yy} \\ \varepsilon_{zz} \end{bmatrix} = \begin{bmatrix} \frac{1}{E_x} & -\frac{v_{yx}}{E_y} & -\frac{v_{zx}}{E_z} \\ -\frac{v_{xy}}{E_x} & \frac{1}{E_y} & -\frac{v_{zy}}{E_z} \\ -\frac{v_{xz}}{E_x} & -\frac{v_{yz}}{E_y} & \frac{1}{E_z} \end{bmatrix} \begin{bmatrix} \sigma'_{exx} \\ \sigma'_{eyy} \\ \sigma'_{ezz} \end{bmatrix} \tag{10}$$

where the index correspondence is 1→x, 2→y, 3→z. The shear strains are not included in equation (10) for simplification, which can be found in Jaeger et al..[27] E_i are Young's moduli in directions $i, i = x, y, z$ denoting the different direction, v_{ij} is Poisson's ratio representing the compression in j direction when a tension is applied in i direction. Young's moduli and Poisson's ratio satisfy the following relationship:[31]

$$\frac{v_{yx}}{E_y} = \frac{v_{xy}}{E_x}, \quad \frac{v_{zx}}{E_z} = \frac{v_{xz}}{E_x}, \quad \frac{v_{zy}}{E_z} = \frac{v_{yz}}{E_y} \tag{11}$$

2.2. Theoretical development of anisotropic permeability

The characteristics of a fracture network influence coal permeability (Fig. 2). Fracture opening, intensity, tortuosity, and connectivity can affect the permeation of fluid through the cross-section. Generally, fluid flow through parallel straight fracture can be captured by cubic law.[32] Considering the effects of fracture intensity, tortuosity, and connectivity, the coal permeability can be expressed as:[33]

$$k = \frac{R_c}{\tau} D_f \frac{a^3}{12} \tag{12}$$

where τ is fracture tortuosity, R_c is fracture connectivity, D_f is fracture intensity and a is the averaged fracture aperture.

The fracture porosity, n_f, can be estimated as:

$$n_f = aA \tag{13}$$

where A is the specific surface area of fractures, defined as the area of total fracture surface per unit volume of coals.

Substituting equation (13) into equation (12) yields:

$$k = \frac{R_c}{\tau} \frac{D_f}{A^3} \frac{n_f^3}{12} \tag{14}$$

Equation (14) can be extended for the ith directional permeability as:

$$k_i = \frac{R_{ci}}{\tau_i} \frac{D_{fi}}{A^3} \frac{n_{fi}^3}{12}, \quad i = x, y, z \tag{15}$$

It can be seen from equation (15) that the fracture permeability in coal is mainly dependent on three factors: fracture distribution characteristics (tortuosity and connectivity), intensity, and size (n_{fi}). It is generally assumed that the fracture distribution characteristics and the fracture intensity coefficients remain constant during fluid flow.[33] However, the fracture porosity varies with the flow.[33] Following work, it is assumed that the fracture porosity is mainly due to change in fracture aperture. On the other hand, fracture closure or opening is associated with variation of stress normal to surface stress.[34] Under true triaxial stress conditions, as shown in Fig. 2, permeability is affected by the variation of each principal stresses[35,36] acting on the coals. Differentiating equation (15) with respect to net stresses in the principal directions and its rearrangement follows:

$$dk_i = \frac{R_{ci}}{\tau_i} \frac{D_i}{A^3} \frac{n_i^3}{4} \sum_{j=x,y,z} \frac{\partial n_{fi}}{n_{fi} \partial \sigma'_{jj}} d\sigma'_{jj}, \quad j = x, y, z \tag{16}$$

where $\sigma'_{jj} = \sigma_{jj} - b_{fjj} p_f$ is defined as the effective stress acting on coal fractures. Here, compression is considered to be positive. It should be noted that the total stresses acting on the porous matrix and the fractures

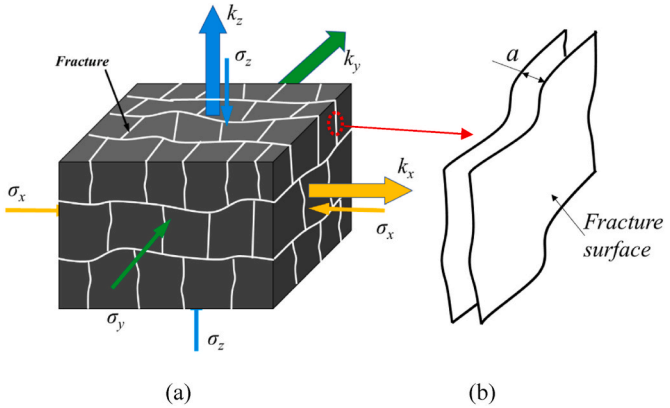

Fig. 2. (a) Schematic of permeability anisotropy of coals and (b) single fracture structure.

are the same, and it can be obtained via the bulk effective stress relationship presented in equation (3).

The directional fracture compressibility is defined as:

$$C_{fij} = -\frac{\partial n_{fi}}{n_{fi}\partial \sigma'_{jj}} \tag{17}$$

Incorporating equations (15) and (17) into equation (16) yields:

$$\frac{dk_i}{k_i} = -\sum_{j=x,y,z} C_{fij} d\sigma'_{jj}. \tag{18}$$

Therefore, the fracture permeability in the ith direction can be obtained by integrating equation (18), and it takes the form:

$$k_i = k_{i0} e^{-3\left(C_{fix}\Delta\sigma'_{xx} + C_{fiy}\Delta\sigma'_{yy} + C_{fiz}\Delta\sigma'_{zz}\right)} \tag{19}$$

where $\Delta\sigma'_{xx} = \sigma'_{xx} - \sigma'_{xx0}$, $\Delta\sigma'_{yy} = \sigma'_{yy} - \sigma'_{yy0}$, $\Delta\sigma'_{zz} = \sigma'_{zz} - \sigma'_{zz0}$, k_{i0} and σ'_{jj0} are fracture permeability and net stress at the reference stress state, respectively.

The directional fracture compressibility, C_{fij}, is not necessarily a constant and is often found to be a function of stress. In addition to the effective stresses, gas adsorption can alter fracture compressibility. Laboratory experiments on gas adsorption in coal revealed that coal-gas interaction can lead to enhancement the coal compressibility.[26,37] McKee et al.[38] presented a stress dependent fracture compressibility relationship, which has been extended here to describe the anisotropic fracture:

$$C_{fij} = \frac{C_{fij0} f_{ai}}{\alpha_{ij}\left(\sigma'_{jj} - \sigma'_{jj0}\right)}\left[1 - e^{-\alpha_{ij}\left(\sigma'_{jj} - \sigma'_{jj0}\right)}\right] \tag{20}$$

where C_{fij0} is the initial fracture compressibility, α_{ij} is the fracture compressibility change rate, and the f_{ai} is a factor representing the adsorption-induced change in compressibility of coal in the ith direction.

Experimental observations provide persuasive evidence that the coal-gas interaction causes severe mechanical degradations in coal, e.g.,[39,40] and this interaction induced mechanical alterations depends on the coal type, adsorbed gases, interaction duration and confining stress.[41] It is believed that gas adsorption can cause fracture walls to be weakened,[41] the reciprocal of fracture compressibility can be assumed to be negatively related to gas adsorption. To consider the dependence of fracture compressibility on factors mentioned above, the following Langmuir-type relationship is proposed to describe the effect of coal-gas interaction on fracture compressibility in this work:

$$\frac{1}{f_{ai}} = 1 - \frac{\sum_{m=1}^{n_g} \gamma_{mi} b_{Lm} x_m p_m}{1 + \sum_{m=1}^{n_g} b_{Lm} x_m p_m} \tag{21}$$

where γ_{mi} is a constant accounting for maximum variation of fracture compressibility due to adsorption-induced weakening effect of mth gas component.

From equation (19) it is evident that the directional permeability can be affected by the change of principal stresses in any direction. This provides a tool to quantify the effects of stresses in all directions on coal permeability. For isotropic conditions, the fracture compressibility is identical in all three directions, which results into a permeability model similar to that of Seidle et al.[42] and Cui and Bustin.[43] In that case, mean stress is used in equation (18). On the other hand, when the effect of only horizontal stress is considered, the model is analogous to the permeability model of Shi and Durucan.[44] However, in their permeability models, the effect of adsorption-induced deformation on permeability is neglected. With respect to CBM extraction, carbon storage and underground coal mining activities, the in-situ stress is generally anisotropic, and a coal seam is likely to be under true triaxial stress conditions.

Please note that the developed anisotropic permeability model requires nine cleat compressibility factors, which can be easily determined from laboratory experiments. The estimation procedure of the nine direction-dependent fracture compressibility will be provided in Section 3.2.2.

3. Model validation

This section presents a series of validation tests to analyse the reliability of proposed models for interpreting anisotropic swelling and permeability behaviour of coals. Relevant experimental data published in the works[15,16,35,45] are used as a benchmark.

3.1. Anisotropic coal swelling

Day et al.[15] used an optical method to directly measure CO_2-induced swelling in three Australian bituminous coals obtained from the Hunter Valley, Illawarra region, and Bowen Basin. The test temperatures varied between 25 and 55 °C, and pressures up to 15 MPa in an incremental manner. Day et al.[15] presented the linear expansion results of Sample 1 from the Hunter Valley, conducted at 40 °C, and reported that the results of the other two samples were identical.

Directional swelling strains of a bituminous coal sample from the Hunter Valley, New South Wales, Australia, were measured by Pan and Connell[16] in a triaxial permeability cell. They measured gas adsorption and permeability under hydrostatic conditions. The radial and axial displacements were measured at each adsorption step to obtain the swelling strain. They measured the directional deformations for different gas species (CO_2, CH_4, N_2). Following Pan and Connell,[16] gas adsorption behaviour is captured by Langmuir isotherm.

Here, the directions parallel to the bedding are set as x- and y-axis, and the direction perpendicular to the bedding is z-axis. The experimental results revealed that the swelling strains in the two directions parallel to the bedding plane are almost the same. Therefore, the mechanical parameter, Young's modulus is assumed to be constant and equal in the x and y directions. In other words, the coal is considered as transversely isotropic. The coal swelling strains were recorded at the equilibrium state; thus, the fluid pressure in coal matrices and fractures are considered to be identical, i.e. $p_m = p_f = p$. Due to lack of information, it is assumed that the effective stress coefficients in three directions are same, i.e. $b_{mii} = b_m$, $b_{fii} = b_f$ (no summation on repeated index here). Since gas adsorption occurs largely in the coal matrix, surface of coal pores mainly depends on coal matrix porosity, thus, $\xi_f = 0$.[8,28] Under an unjacketed experimental condition ($\sigma_{ii} = -p$). Therefore, the effectives stresses in the three axis directions are reduced to:

$$\sigma'_{eii} = (b-1)p + \Psi RT\ln(1 + pb_L) \tag{22}$$

where $b = b_m + b_f$, $\Psi = b_m \xi_m I^{max}$. Equation (22), in combination with equation (10) are solved analytically to calculate swelling strains of the coal samples. The model parameters obtained from the validation exercises are listed in Table 1. Pan and Connell[16] developed an anisotropic coal swelling model (P–C model) to match these experimental data. And it is shown that the estimated values of Young moduli and Poison's ratio

Table 1
Parameters for validation test of the developed anisotropic swelling model.

Data source	Day et al.[15]	Pan and Connell[16]		
Swelling model	This Study	This Study		
Species	CO_2	CO_2	CH_4	N_2
Langmuir pressure constant, b_L, MPa^{-1}	1.16	0.93	0.79	0.27
Surface stress constant, Ψ, mol/m^3	5508	11693	6017	4007
Young's modulus, E_x, GPa	2.1	1.3		
Young's modulus, E_y, GPa	2.1	1.3		
Young's modulus, E_z, GPa	1.5	0.95		
Poison's ratio, ν_{yx}	0.23	0.30		
Poison's ratio, ν_{zx}	0.31	0.44		
Poison's ratio, ν_{zy}	0.31	0.44		
Effective stress coefficient, b	0.48	0.95		

in all directions are very closed to those obtained by Pan and Connell[16] for both Day et al.'s data and Pan and Connell's data.

The model predicted swelling strains are compared against the results of Day et al.[15] and Pan and Connell[16] in Fig. 3 and Fig. 4, respectively. The predicted results agree well with both experimental measurements indicating that the proposed swelling model can describe adsorption-induced anisotropic coal deformation behaviour both quantitatively and qualitatively. In all cases, expansion in the direction perpendicular to the bedding plane is greater than that in the parallel plane. For example, in Fig. 3, at 10 MPa CO_2 pressure, swelling strain in the direction parallel to the bedding plane is approx. 0.52%. Whereas in the perpendicular direction it is 0.82%, an increase of 57.6% in swelling strain.

Adsorption-induced swelling strain behaviour of coal is gas species dependent, as illustrated in Fig. 4. More CO_2 generally adsorbs in coal than CH_4 or N_2. From equation (6), it can be shown that the reduction of surface stress due to the adsorption of CO_2 is more significant than CH_4 or N_2. This is why coal exhibits larger swelling strain in contact with CO_2 than CH_4 and N_2.

In order to evaluate the performance of developed anisotropic model, the presented swelling model and the P–C model are tested against experimental results and are presented in Fig. 5. The experimental data by Pan and Connell[16] for CO_2 are used as the benchmark. The parameters for P–C model are listed in Table 2. Compared to P–C model, the number of required parameters for the proposed model is reduced. It can be seen from Fig. 5 that both models underestimate swelling strain when pressure is lower and overestimate for higher pressure. A possible cause for these differences is that estimated surface stress constant for proposed model and Langmuir volume constant for P–C model are an average over the whole pressure range, the values for higher pressure may be overestimated because compression of coal due to higher pressure could reduce gas adsorption.[46] In comparison, P–C model show slightly better fitting when pressure ranges from 2 to 6 MPa. However, when pressure is higher, the deviation of P–C model from experimental results is significantly more than that of the proposed model in this study.

3.2. Anisotropic and isotropic permeability

3.2.1. Robertson's permeability data (isotropic)

In this work, a weakening coefficient is introduced in the permeability model, for the first time, to explain the effect of change in mechanical properties of fractures due to gas adsorption and permeability evolution. Its rationality can be examined via experimental measurements of coal permeability under stress controlled conditions. Most the laboratory tests on coal permeability evolution for varied pressures or varied confining stresses were conducted in one direction, e.g.[37,45,47]

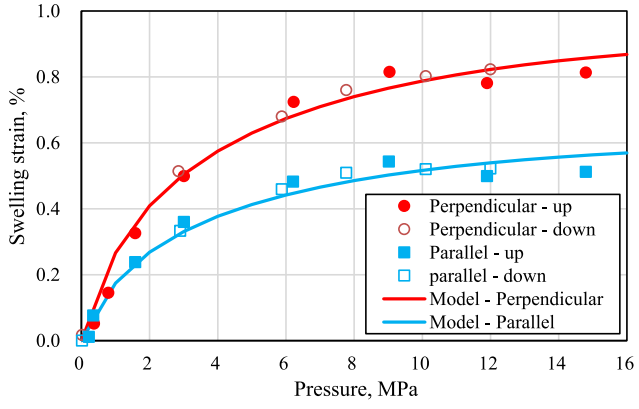

Fig. 3. Comparison between the experimental data of Day et al.[15] and predicted swelling strain.

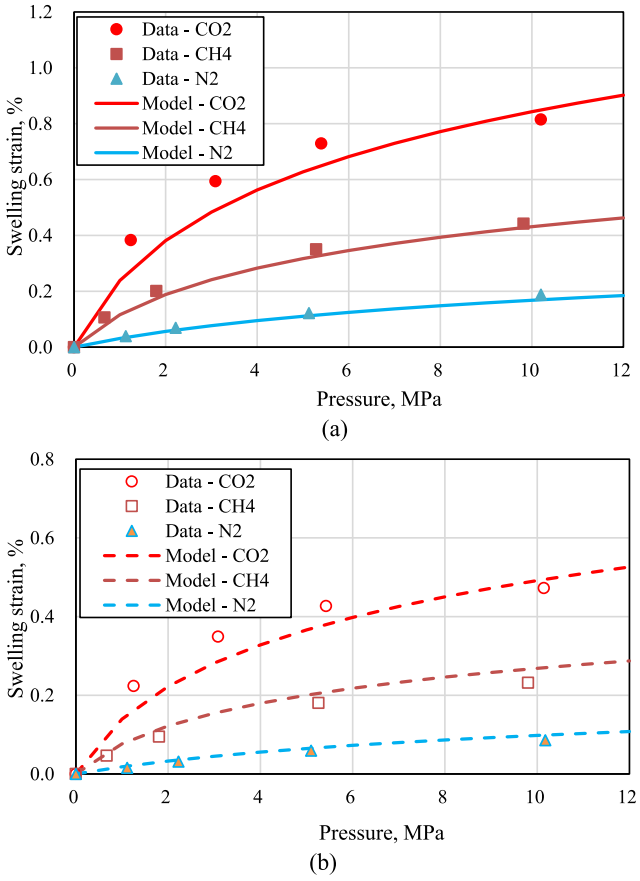

Fig. 4. Comparison between the experimental data of Pan and Connell[16] and predicted swelling strain: (a) perpendicular to the bedding and (b) parallel to the bedding.

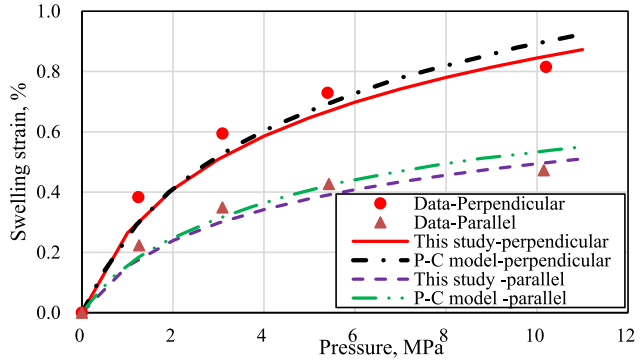

Fig. 5. Comparisons of different anisotropic swelling model results with the experimental data for CO_2.

Table 2
Parameters for matching anisotropic swelling data with P–C model.

Langmuir pressure constant, b_L, MPa^{-1}	0.83	Porosity, n,-	8.9%
Langmuir volume constant, L, mol/kg	1.76	Coal density, ρ_s, kg/m^3	1470
Young's modulus, E_x, GPa	1.4	Length, l_x, m	0.5
Young's modulus, E_y, GPa	1.4	Length, l_z, m	0.5
Young's modulus, E_z, GPa	0.95	Length, l_z, m	0.4
Poison's ratio, ν_s	0.47		

Note: These parameters are only for Pan and Connell's model.

Robertson[45] performed two sets of experimental tests on coal permeability to investigate, firstly, the effect of confining stress on coal permeability by keeping gas pressure constant but varying confining stress (same confining pressure to all surfaces of the cores); and secondly, the effect of gas pressure on coal permeability by keeping confining pressure constant and by varying gas pressure. The details are available in Robertson.[45] The experimental results for one coal sample, Anderson 01, are used as benchmark for this validation test. When confining pressure varies but holding gas pressure remains constant, the permeability model is reduced to the following form:

$$k_x = k_{x0} e^{-3\left[\left(C_{fxx}+C_{fxy}+C_{fxz}\right)\left(\sigma_c-\sigma_{c0}\right)\right]} \tag{23}$$

However, when the confining pressure is constant, the permeability model for varying gas pressure can be expressed as:

$$k_x = k_{x0} e^{-3\left[\left(C_{fxx}+C_{fxy}+C_{fxz}\right)\left(\sigma_{c0}-b_f p\right)\right]} \tag{24}$$

Here, σ_c is confining pressure.

The parameters used in this analytical validation test are listed in Table 3. The coal sample is assumed to be isotropic, i.e. $C_{fxx} = C_{fxy} = C_{fxz} = C_f$. The permeability results obtained from the experimental tests with varying confining stress are used to estimate the initial fracture compressibility and fracture compressibility change rate. Following that the experimental data of different gases (CO_2, CH_4, and N_2) are used to estimate the weakening coefficient. Langmuir pressure constants for different gases are chosen from Chen et al..[8] The validation results are presented in Fig. 6. To keep consistent with experimental results presented by Robertson,[45] when considering the effect of confining stress on coal permeability, the permeability tested at net stress of 900 psi is selected as a basis to show the variation of permeability, as shown in Fig. 6(a). When considering the effect of gas pressure on coal permeability, the permeability of coal at gas pressure 100 psi are selected as a basis for CO_2, N_2 and CO_2/N_2 mixture, as shown in Fig. 6 (b, d, e), while the permeability of coal tested at gas pressure 72 psi are selected as a basis for CH_4, as shown in Fig. 6 (c). The accuracy of the proposed model results is compared to the fitting results of both Shi-Durucan model (S-D model) and the Palmer-Mansoori model (P-M model) in Fig. 6.

Compared to predictions of both S-D model and P-M model, there is a better agreement between the experimental measurements and predictions of the permeability model proposed in this work (see Fig. 6). More importantly, the proposed model can describe the coal permeability evolution induced by different gas species and gas mixture using a common set of coal properties. It is shown that the coal permeability decreases as the confining stress increases. At constant confining stress, the coal permeability decreases with gas pressure, reaches to a minimum, and thereafter, starts to rebound. This is because with increasing effective stress the fracture compressibility reduces, which is shown in Fig. 7 for various gases. It is observed that the change in compressibility is species dependent. The fracture compressibility undergoes a nearly linear increase with gas pressure due to combined effects of effective stress decrease and gas adsorption induced structural alteration. For example, it was shown when gas pressure increases from 0.67 MPa (100 psi) to 5.5 MPa (800 psi), the fracture compressibility for CO_2 increases from 0.073 MPa^{-1} (0.0005 psi^{-1}) to 0.20 MPa^{-1} (0.00138 psi^{-1}). Similar findings were also reported in Pan et al.[37] and Peng et al.[26] For example, Pan et al.[37] reported that the fracture compressibility of coals for CO_2 increased from 0.05 MPa^{-1} to 0.125 MPa^{-1} with pressure. It can be seen that compressibility increases for CO_2 are comparable to those presented in Pan et al.[37]

This finding can be used to explain why coal permeability continue to decrease although the net stress for fractures decreases. At lower gas pressures, although the net stress acting on fractures is reduced, the fracture compressibility increases due to gas adsorption induced coal structure change, and the fractures can be compressed at this stage. However, with an increase in gas pressure, the impact of gas pressure becomes dominant and the fractures re-open, resulting in an increase of coal permeability, as shown in Fig. 5. This can explain why coal permeability continue to decrease although the net stress for fractures decreases.

Table 3
Parameters for validating Robertson's[45] permeability test.

Parameters	CO_2	CH_4	N_2
Langmuir pressure constant, b_L, psi^{-1}	0.0061	0.0046	0.002
Weakening coefficient, γ_m, -	0.66	0.48	0.4
Initial fracture compressibility, C_{f0}, psi^{-1}	9.5e-4		
Fracture compressibility change rate, α, psi^{-1}	0.0025		
Biot's coefficient, b_f	0.8		

3.2.2. Duan et al.'s permeability data (anisotropic)

Experimental data of Duan et al.[35] are used to examine the accuracy of the presented anisotropic permeability model. Duan et al.[35] investigated the influence of anisotropy of coal structure and stress state on permeability evolution using a multifunctional true triaxial geophysical apparatus. They carried out mechanical and seepage experiments on cubic coal samples of 100 mm × 100 mm × 100 mm dimensions. Permeability of the coal samples in three directions under true triaxial stress conditions was tested. Nine different experimental conditions were designed to consider different stress conditions and flow directions, as shown in Fig. 8. There are three kinds of loading path: 1) minimum principal stress is perpendicular to bedding, 2) intermediate principal stress is perpendicular to bedding and 3) maximum principal stress is perpendicular to bedding. For each loading path, the maximum stress of 50 MPa and minimum stress of 10 MPa were kept constant, and the intermediate stress was increased from 10 to 50 MPa step by step. Flow in each direction was tested with three different loading paths. In following, the designed flow in x direction with three loading paths are defined as L1F1, L2F1, L3F1, flow along the direction y as L1F2, L2F2, L3F2 and flow along direction z as L1F3, L2F3, L3F3.

Equation (19) is used to predict the coal permeability variation in each direction. The model parameters are estimated by fitting the experimental results. Fig. 9 shows the estimated material parameters including initial permeability in three directions and anisotropic compressibility. The permeability was tested with a low, constant gas pressure of 1 MPa. Change in loading is the only factor that affects the evolution of permeability. Due to the low permeability of the coal samples, the compressibility is assumed to be constant. In this validation test, the permeability data for L1F1, L2F1 and L3F1 are used for estimation of the initial permeability in the x-direction, and compressibility C_{fxx}, C_{fxy}, C_{fxz}. The permeability data for L1F2, L2F2, L3F2 for the initial permeability in the y-direction, and compressibility C_{fyx}, C_{fyy}, C_{fyz}. The permeability data under L1F3, L2F3, L3F3 for initial permeability in the z-direction, and compressibility C_{fzx}, C_{fzy}, C_{fzz}. The estimated initial permeability in all directions is the permeability at unstressed conditions.

The same coal sample was used for all tests under different flow indirection and stress condition, loading and unloading for each test could cause the slight loss of permeability due to irreversible permeability. Thus, the estimated parameters may deviate slightly from their actual value From Fig. 9(a), the estimated initial permeability in the x-direction is between 1.16 and 2.38 times greater than in y- and z-directions in this experiment. Fig. 9(b) shows that the estimated compressibility values related to stress applied perpendicularly to the bedding, are larger than the flow parallel to the bedding. This implies that the permeability parallel to the bedding is more sensitive to change in stress perpendicular to the bedding. In addition, it can be observed that when the flow direction is identical to the applied stress direction, the compressibility is lower, especially in the direction parallel to the bedding, while it is higher for stress vertical to flow direction. For example, when flow is along the x-cleat direction, the compressibility

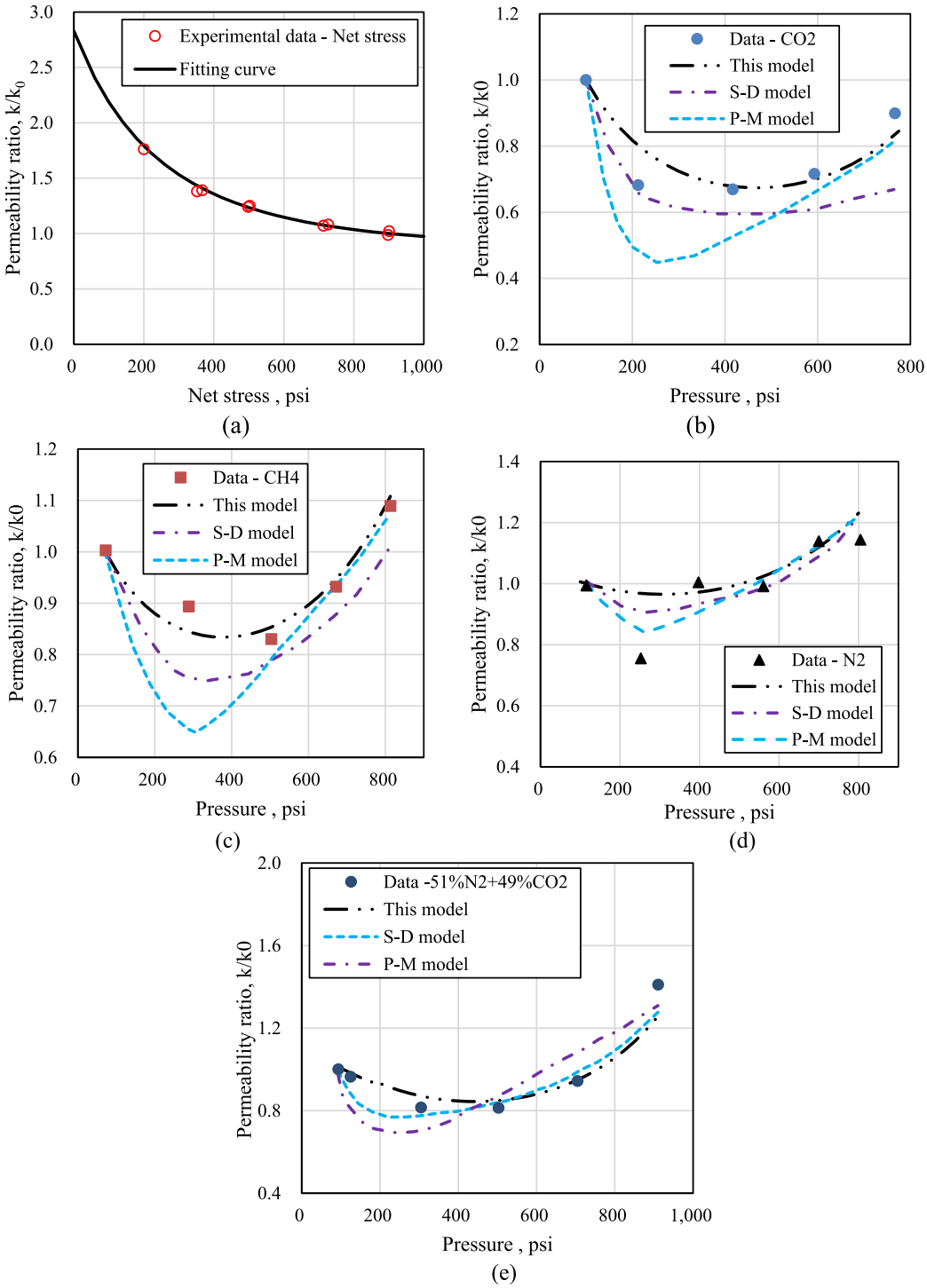

Fig. 6. Performances of different coal permeability models against experimental data of 'Anderson 01' coal sample by Robertson[45]: (a) varying confining stress, (b–e) varying gas pressure, (b) CO_2, (c) CH_4, (d) N_2, (e) 51%N_2+49%CO_2.

C_{fxx} is 0.001 MPa^{-1} but C_{fxy} is 0.0052 MPa^{-1}. None of the compressibility parameters is estimated to be zero indicating that the permeability is affected by the stress in all directions.

Fig. 10 compares the predicted responses with the experimental data of coal permeability from Duan et al.[35] It can be seen from Fig. 10 that the permeability evolution predicted by the model achieved a good agreement with the observations from the experimental test. Which is indicative of the reliability and effectiveness of the model. Duan et al.[35] presented an anisotropic permeability model to match their experimental results. The matching results of Duan et al.'s model and the proposed model in this study are compared, as shown in Fig. 11. The experimental data for L1F1, L2F1 and L3F1 are used for benchmark. As expected, Fig. 11 shows that the Duan et al.'s model overestimates coal permeability, in contrast, the proposed model shows a better match.

4. Results and discussions

Boundary conditions can significantly influence coal permeability behaviour. In this section, the presented model has been applied to investigate the effect of anisotropic deformation on coal permeability

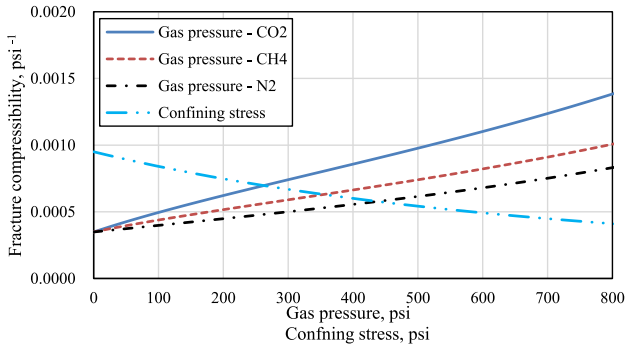

Fig. 7. Fracture compressibility of coal with respect to confining stress and gas pressure for different gases.

under various boundary conditions including constant volume conditions, uniaxial strain condition, and plane strain condition. The estimated mechanic properties from validation tests with experimental results of Pan and Connell[16] and Duan et al.[35] as a benchmark are used in these cases, as listed in Table 4 and Fig. 9. The permeability ratio is used to evaluate the change in permeability with pressure at equilibrium state, i.e. $p_m = p_f = p$.

Case 1: Constant volume condition

Under constant volume conditions, the vertical and horizontal strains are equal to zero, i.e.

$$\varepsilon_{xx} = \varepsilon_{yy} = \varepsilon_{zz} = 0 \tag{25}$$

Substituting equation (25) into equation (10) yields the effective stresses for bulk coal due to volume constrain, and it is expressed as:

$$\sigma'_{exx} = \sigma'_{eyy} = \sigma'_{ezz} = 0 \tag{26}$$

Inserting equation (26) into equation (3) and combing with equation (18), the changes in effective stresses only acting on fractures can be given as:

$$\Delta\sigma'_{xx} = \Delta\sigma'_{yy} = \Delta\sigma'_{zz} = b_m\Delta p - b_m\Delta p^s_m \tag{27}$$

Combining equation (27) with equation (19) and equation (8), the coal permeability with pressure is obtained. Equation (27) indicates the change in coal permeability is not related to the coal mechanical properties but only to pressure, the anisotropic coal swelling cannot affect the anisotropic coal permeability. The response curves of coal permeability for pure gas and gas mixture are shown in Fig. 12 and Fig. 13.

Fig. 12 shows that coal permeability in all directions undergoes a significant decrease at a lower pressure when coal is completely constrained. For example, the permeability drops by about 83% in *x*-direction, 80% in *y*-direction and 63% in *z*-direction when pressure reaches 4 MPa. However, with increase of pressure, the permeability decease slows down. This is because the coal swelling increases quickly with pressure when it is lower, as shown in Figs. 3 and 4. When the pressure is higher, the increase of coal swelling is marginal. When the gas mixture is used as interacted gases, although the coal permeability shows a decrease, this decrease is lessened compared to the variation of coal permeability with pure gas, as illustrated in Fig. 13. The higher the fractionation of N_2 in the gas mixture, the lesser the decrease of coal permeability. When N_2 takes up 80% of the gas mixture, the coal permeability drops by approximately 50% in *x*- and *y*-directions and 33% in the *z*-direction. The CO_2 adsorption-induced coal swelling is greatly larger than that of N_2 in coal. An increase in the fraction of N_2 in

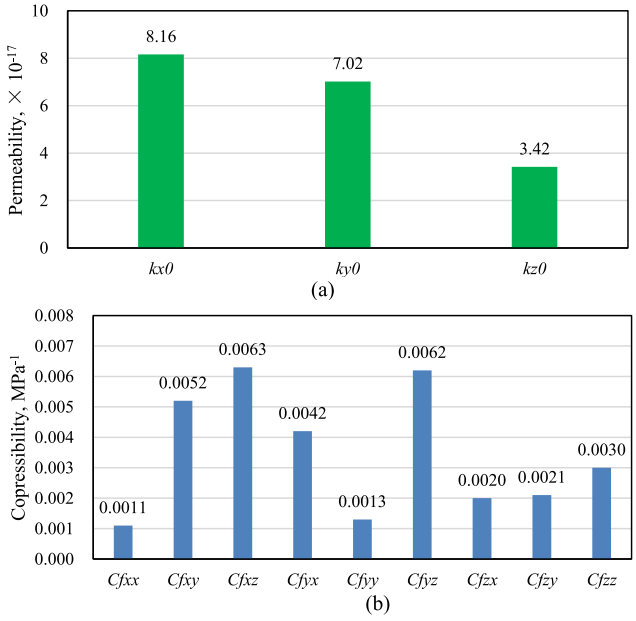

Fig. 9. (a) Estimated initial permeability in three directions and (b) the anisotropic compressibility to match experimental data.

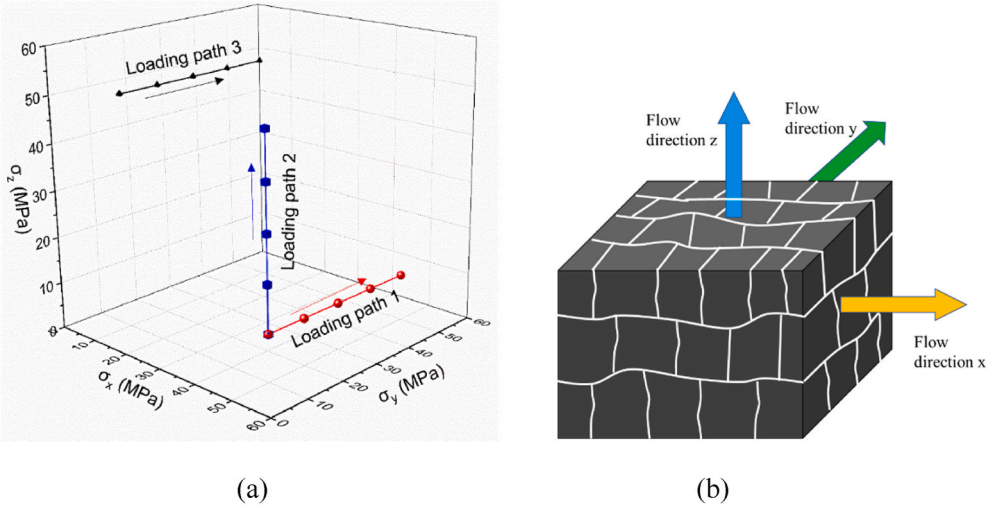

Fig. 8. (a) Designed stress loading paths and (b) flow directions in Duan et al.'s experimental tests.

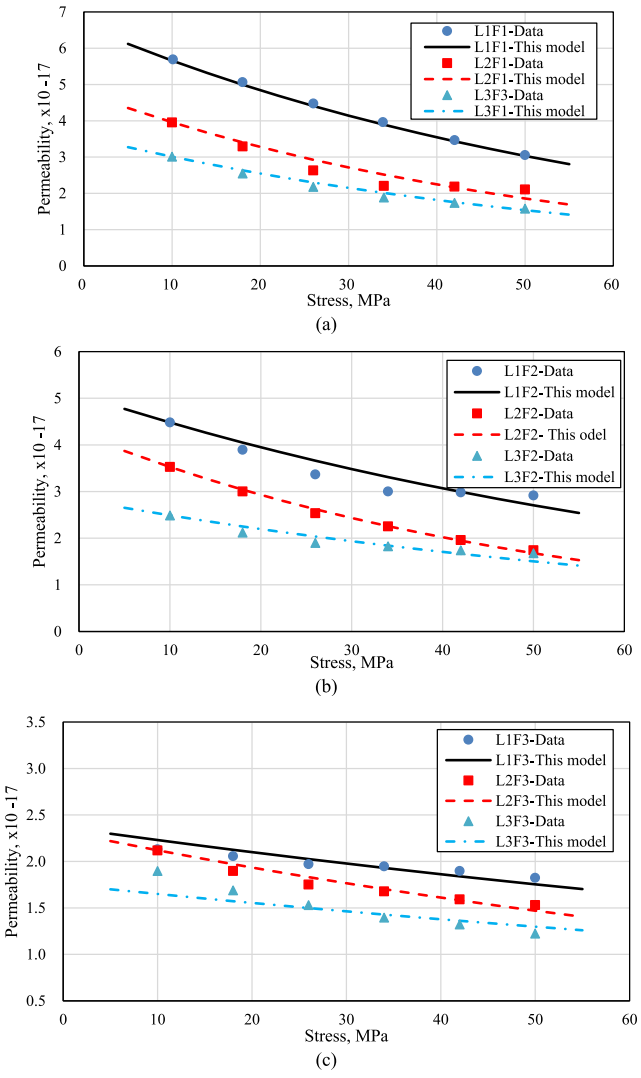

Fig. 10. Comparisons of measured permeability and model prediction under different stress conditions and flow directions: (a) L1F1-L3F1, (b) L1F2-L3F2 and (c) L1F3-L3F3.

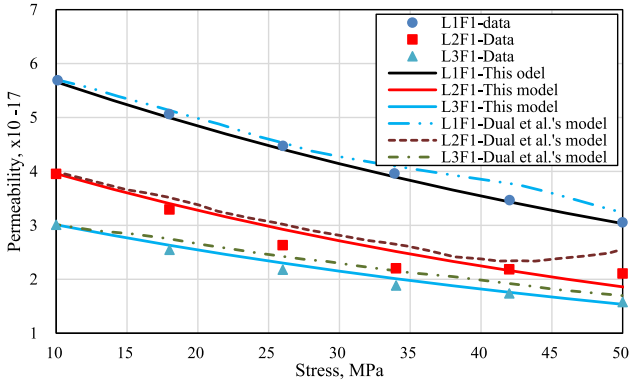

Fig. 11. Comparisons between matching results of different permeability models.

Table 4
Parameters for investigation of anisotropic coal permeability.

Parameters	Values
Temperature, T, K	303
Young's modulus, E_x, GPa	1.3
Young's modulus, E_y, GPa	1.3
Young's modulus, E_z, GPa	0.95
Poison's ratio, ν_{yx}	0.32
Poison's ratio, ν_{zx}	0.44
Poison's ratio, ν_{yz}	0.44
Surface stress constant for CO_2, Ψ, mol/m^3	11693
Surface stress constant for N_2, Ψ, mol/m^3	4007
Langmuir pressure constant for CO_2, b_L, MPa^{-1}	0.93
Langmuir pressure constant for N_2, b_L, MPa^{-1}	0.27
Effective stress coefficient, b, -	0.95
Effective stress coefficient, b_m, -	0.1

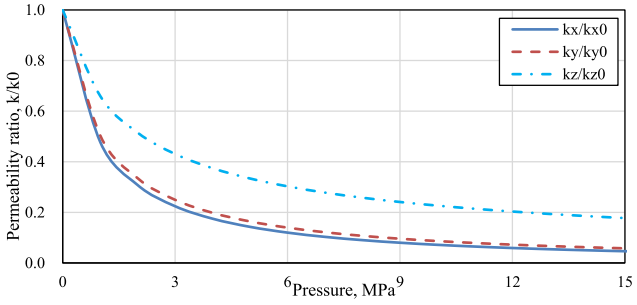

Fig. 12. Permeability evolution of coal with pure gas under constant volume condition.

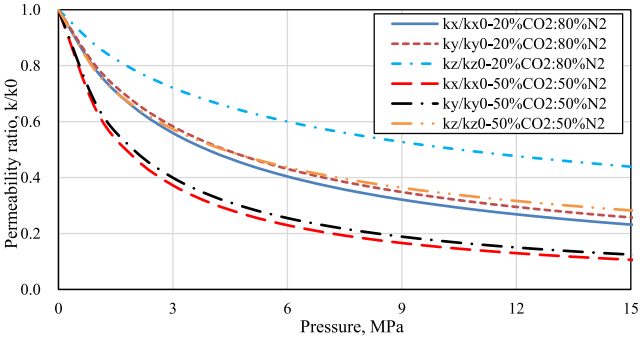

Fig. 13. Permeability evolution of coal with a mixture of gases under constant volume condition.

the gas mixture will lead to a decrease in coal swelling. This is why the permeability of coal with gas mixture shows a relatively less reduction of its value.

To examine the predicted coal permeability with gas pressure, the laboratory tests were collected for comparison. Due to the fact that most of the experiments on coal permeability with gas pressure were conducted under constant confining pressure, or constant pressure difference between confining pressure and gas pressure, and permeability in only one direction were tested. In comparison, the permeability data tested under constant pressure difference conditions may be used to approximate the evolution of permeability under constant volume conditions. We collected the experimental data from literatures,[48–55] as shown in Fig. 14. The permeability ratio is defined as the ratio of

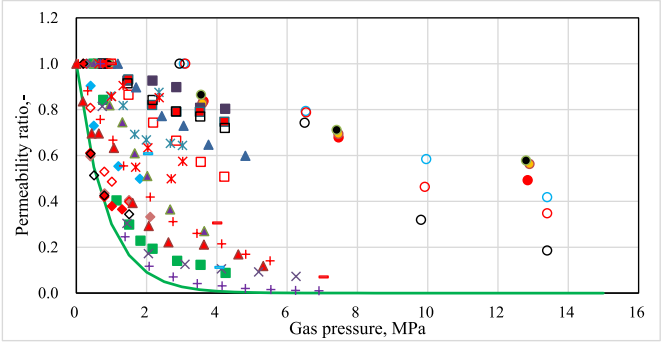

Fig. 14. Statistics of experimental data on coal permeability under constant pressure difference conditions, symbols with same shape means data collected from same work: circle (o) represents data from Chen et al.,[49] square (□) from Lin et al.,[48] diamond (◇) from Li et al.,[50] triangular (△) from Lin and Kovscek,[51] cross (+) from Mira et al.,[52] star (Ж) from Semoon et al.,[53] plus (+) from Ma et al.,[54] minus (−) from Meng and Li.[55].

permeability at the resting pressure to that at the initial pressure. As seen in Fig. 14, permeability of coal in all experiment tests experiences a significant drop with pressure, especially when pressure is lower. Model predicted permeability evolution above are similar to experimental tests and fall within the range of tested permeability ratio, which indicates the capacity of the permeability model for the predictive purpose.

Case 2: Uniaxial strain condition

The uniaxial strain condition is widely used for reservoir boundary conditions where the zero lateral or horizontal strains are assumed everywhere in the domain, i.e.

$$\varepsilon_{xx} = \varepsilon_{yy} = 0 \tag{28}$$

Substitution of equation (28) into equation (10) and solving equation (10) yields effective stress:

$$\sigma'_{exx} = \frac{E_x}{E_z}\frac{v_{zx} + v_{zy}v_{yx}}{1 - v_{yx}v_{xy}}\sigma'_{ezz} \tag{29}$$

$$\sigma'_{eyy} = \frac{E_y}{E_z}\frac{\left(v_{zy} + v_{xy}v_{zx}\right)}{1 - v_{yx}v_{xy}}\sigma'_{ezz} \tag{30}$$

Combining equations (29) and (30) with equations (3) and (18), the changes in effective stresses acting on fractures can be given as

$$\Delta\sigma'_{xx} = b_m\Delta p - b_m\Delta p^s_m - \frac{E_x}{E_z}\frac{v_{zx} + v_{zy}v_{yx}}{1 - v_{yx}v_{xy}}\left(-\Delta\sigma_{zz} + b\Delta p - b_m\Delta p^s_m\right) \tag{31}$$

$$\Delta\sigma'_{yy} = b_m\Delta p - b_m\Delta p^s_m - \frac{E_y}{E_z}\frac{\left(v_{zy} + v_{xy}v_{zx}\right)}{1 - v_{yx}v_{xy}}\left(-\Delta\sigma_{zz} + b\Delta p - b_m\Delta p^s_m\right) \tag{32}$$

It is further assumed that the overburden stress remains unchanged in reservoirs, i.e. $\Delta\sigma_{zz} = \sigma_{zz} - \sigma_{zz0} = 0$, equations (31) and (32) are written as:

$$\Delta\sigma'_{xx} = b_m\Delta p - b_m\Delta p^s_m - \frac{E_x}{E_z}\frac{\left(v_{zx} + v_{zy}v_{yx}\right)}{1 - v_{yx}v_{xy}}\left(b\Delta p - b_m\Delta p^s_m\right) \tag{33}$$

$$\Delta\sigma'_{yy} = b_m\Delta p - b_m\Delta p^s_m - \frac{E_y}{E_z}\frac{\left(v_{zy} + v_{xy}v_{zx}\right)}{1 - v_{yx}v_{xy}}\left(b\Delta p - b_m\Delta p^s_m\right) \tag{34}$$

and

$$\Delta\sigma'_{zz} = -b_f\Delta p \tag{35}$$

Substitution of equations (33)–(35) into equation (19) can generate permeability with pressure. Existing permeability models in literature for uniaxial strain conditions, consider that fluid pressure can changes stresses only in the vertical direction, and neglect the effects of vertical coal swelling.[43,44,56] However, in the presented model, the vertical swelling is considered via equations (33)–(35). It can be seen from the equations that under uniaxial strain conditions, stress change is not only associated with coal-gas interaction but also with the mechanical properties of coal. To investigate the impacts of mechanical properties, e.g. Young's moduli and Poisson's ratio that are determined by fitting anisotropic swelling data of Pan and Connell[16] and Day et al.[15] in the previous section, are used to calculate the permeability ratio, and the results are shown in Fig. 15 and Fig. 16. It can be observed that the permeability increases with pressure using the data of Pan and Connell.[16] However, when the mechanical properties data of Day et al.[15] is applied, the coal permeability experiences an initial drop with the pressure, reaches to a minimum, and then start to increase with pressure. The observed rebound behaviour in the data of Day et al.[15] is not present in that of the Pan and Connell.[16] Due to larger Poisson's ratio and role of vertical swelling in the data of Pan and Connell,[16] the increase of compressive stress in *x*- and *y*-directions is smaller. Also, the compressive stress in the vertical direction is reduced by gas pressure and vertical swelling, resulting in a negligible decrease in coal permeability. In contrast, the Poisson's ratio of coal from the data of Day et al.[15] is relatively smaller. The compressive stress in *x*- and *y*-direction initially experiences a larger increase with pressure, and therefore, the coal permeability decreases. As the pressure increases, the increase of stress slows down and the fracture pressure elevates and reopen the fracture. This leads to a recovery of the coal permeability.

The permeability data tested under constant confining stress were collected to calibrate the model predictions since these experiments involve constant stress boundary. These data were collected from works[45,47,57–60] and plotted in Fig. 17. It can be seen although the experimental permeability ratios may increase or decrease with pressure, they fall within a lower bound and an upper one. The permeability evolution trends of coals predicted by the proposed model (Figs. 15 and 16) are consistent with experimental measurements, indicating the reliability of the proposed model.

Case 3 Plane strain condition

Coal seams are usually horizontal or sub-horizontal, and are confined by much harder and thicker rock strata on the top and on the floor. Thus, the predominant deformation occurs in the horizonal direction. The vertical deformation, therefore, can be constrained, i.e.

$$\varepsilon_{zz} = 0 \tag{36}$$

Inserting equation (36) into equation (10) gives:

$$\sigma'_{ezz} = \frac{E_z v_{xz}\sigma'_{exx}}{E_x} + \frac{E_z v_{yz}\sigma'_{eyy}}{E_y} \tag{37}$$

By assuming that the external stresses in *x*- and *y*-direction are

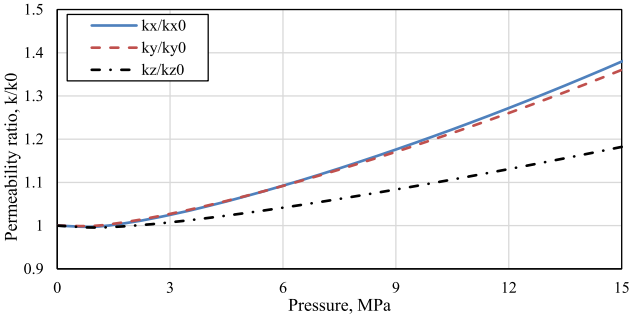

Fig. 15. Permeability evolution of coal used in Pan, Connell[16] under uniaxial strain condition.

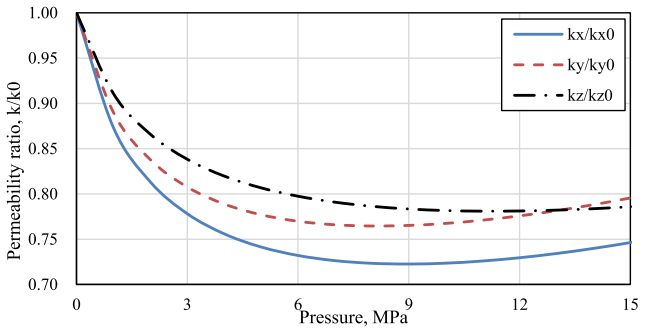

Fig. 16. Permeability evolution of coal used in Day et al.[15] under uniaxial strain condition.

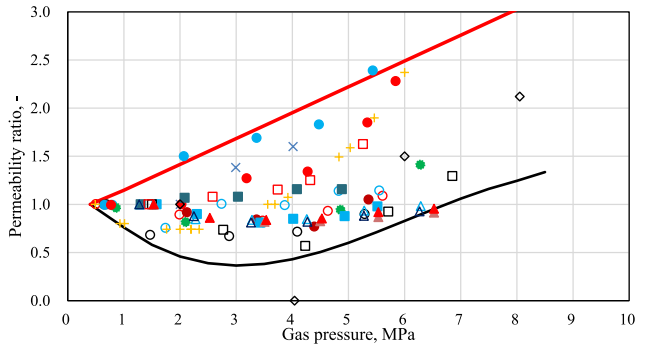

Fig. 17. Experimental data on coal permeability under constant confining stress, symbols with same shape means data collected from same work: cross (X) represents data from Anggara et al.,[57] circle (o) from Robertson,[45] plus (+) from Pini et al.,[47] squares (□) from Kumar et al.,[58] triangular (△) from Li et al.,[59] diamond (⋄) from Niu et al.[60].

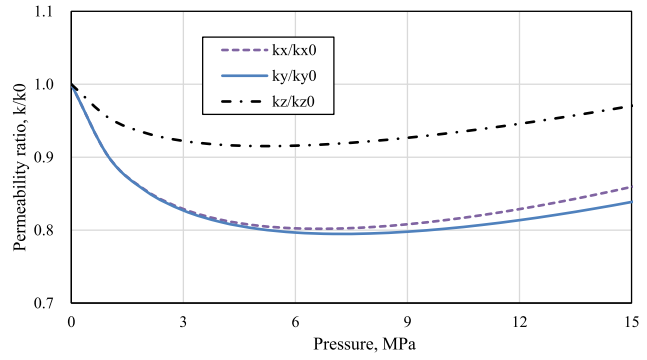

Fig. 18. Permeability evolution of coal under plane strain condition.

constant, the changes in effective stress acting on fractures can be expressed as:

$$\Delta\sigma'_{xx} = \Delta\sigma'_{yy} = -b_f \Delta p \tag{38}$$

$$\Delta\sigma'_{zz} = b_m \Delta p - b_m \Delta p^s_m - \left(\frac{E_z v_{xz}}{E_x} + \frac{E_z v_{yz}}{E_y}\right)\left(b\Delta p - b_m \Delta p^s_m\right) \tag{39}$$

Coal permeability can be obtained by substitution of equations (38) and (39) into equation (19). Similar to uniaxial conditions, the coal permeability evolution is also influenced by mechanical properties of coal. Because the Young's modulus in the vertical direction is generally smaller than that in the horizonal direction and the Poisson's ratio cannot surpass 0.5. Therefore, gas pressure and adsorption-induced swelling could result in an increase of compression stress in the vertical direction.

Fig. 18 shows the varied trend of coal permeability in all directions as pressure increases, the mechanical properties of coal from Pan and Connell[16] are used in calculation of coal permeability. Compared to the continuous increase of permeability shown in Fig. 15, the permeability in the plane strain model decreases initially with pressure, due to displacement constrain in vertical stress. However, the swelling is slow when gas pressure is larger, and the increased pressure can reopen the fracture, which leads to the rebound of coal permeability. Compared to the experimental results shown in Fig. 17, the predicted permeability evolution is similar to experiment results.

5. Conclusions

In this study, an adsorption-induced anisotropic coal swelling and permeability model is presented. The model is developed by combining gas adsorption thermodynamics with anisotropic material properties. A stress-dependent directional permeability model is proposed to represent the anisotropy of coal permeability, in which a direction-related fracture compressibility factor is incorporated. A weakening coefficient is introduced to estimate the impact of gas adsorption on fracture compressibility. The accuracy and reliability of the proposed model are examined via a series of validation exercises against laboratory coal swelling and permeability data along with comparisons between presented and existing models. In all cases, the model predictions exhibit good agreement with the experimental data. The major findings are summarized as follows:

(1) Gas adsorption induced coal swelling in the direction perpendicular to the bedding plane is greater than that in the parallel plane. Fracture compressibility may increase due to coal-gas interaction and CO_2 can cause a larger increase in fracture compressibility compared to CH_4 and N_2.
(2) Although coal permeability in any direction can be influenced by the stress changes in all directions, permeability parallel to the bedding plane is more sensitive to stress changes than that of the perpendicular to the bedding plane, especially change in stress perpendicular to the bedding plane.
(3) Under constant volume condition, coal permeability drops significantly and no rebound was observed, however, coal permeability may rebound with pressure increase under uniaxial strain condition and plane strain condition. Anisotropic swelling and mechanical properties of coal can affect coal permeability anisotropy.
(4) The decrease of coal permeability in direction parallel bedding plane is more significant than that in the direction perpendicular to the bedding plane.

Declaration of competing interest

The authors declare that they have no known competing financial interests or personal relationships that could have appeared to influence the work reported in this paper.

Acknowledgement

The research was conducted as part of the "Establishing a Research Observatory to Unlock European Coal Seams for Carbon Dioxide Storage (ROCCS)" project. The ROCCS project has received funding from the Research Fund for Coal and Steel under Grant Agreement No. 899336. The financial support is gratefully acknowledged.

Appendix. Effective stress for fractured porous media saturated with adsorptive fluids

The detailed procedure of incorporating the thermodynamics of gas adsorption in the anisotropic effective stresses is presented here. As Fig. 1, the media under consideration is comprised of four phases: the solid, bulk fluids in fracture, and the pores, and the adsorptive fluid that is present at the interface between the solid and the fluid. Therefore, the energy balance equation for per unit volume of such a system can be expressed as:

$$dF = dF_s + dF_f + dF_{surf} \tag{A1}$$

Under the assumption of isothermal and infinitesimal deformation, the energy balance at equilibrium for a unit volume of fractured porous media with its fluids can be written as:[28]

$$dF = \sigma_{ij} d\varepsilon_{ij} + \mu_m d\rho_m + \mu_f d\rho_f \tag{A2}$$

When coal is exposed to gases, such as, CO_2 and CH_4, they mostly adsorb onto the surface of matrix pores. It is therefore considered that only bulk phase gas resides in coal fractures, while both bulk phase and adsorbed phase gases coexist in the matrix pores. Thus,

$$\rho_m = \rho_m^b + \rho_m^a \tag{A3}$$

The Helmholtz free energy of the fluids in, a bulk state, per unit volume is:

$$F_f = \mu_m \rho_m^b - n_m p_m + \mu_f \rho_f - n_f p_f \tag{A4}$$

Therefore,

$$dF_f = \rho_m^b d\mu_m + \mu_m d\rho_m^b - p_m dn_m - n_m dp_m + \rho_f d\mu_f + \mu_f d\rho_f - p_f dn_f - n_f dp_f \tag{A5}$$

Applying the Gibbs–Duhem relations,[61] $\rho_m^b d\mu_m = n_m dp_m$ and $\rho_f d\mu_f = n_f dp_f$, equation (A5) can be simplified as:

$$dF_f = \mu_m d\rho_m^b - p_m dn_m + \mu_f d\rho_f - p_f dn_f \tag{A6}$$

Work can be provided to the fluid-solid interface either by increasing its area (working against the surface stress) or by adding more adsorbed molecules. So, the energy balance for the interface is expressed as:[62]

$$dF_{surf} = \sigma^s dA_p + \mu_m d\rho_m^a \tag{A7}$$

The surface of coal pores depends on coal matrix porosity and the volumetric strain of coal matrix,[28] and expressed as:

$$A_p = A_p(\varepsilon_{vm}, n_m) \tag{A8}$$

Considering the macroscopic strain of coal being the space average of coal matrix and fractures,[28] i.e.:

$$\varepsilon_v = (1 - n_{f0})\varepsilon_{vm} + n_f - n_{f0} \tag{A9}$$

where $\varepsilon_v = \varepsilon_{11} + \varepsilon_{22} + \varepsilon_{33}$ is volumetric stain of bulk coal and n_{f0} is fracture porosity in the reference state.

Therefore, equation (A8) can be rewritten as:

$$A_p = A_p(\varepsilon_v - n_f, n_m) \tag{A10}$$

From equation (A1), the change in free energy of the coal without bulk fluids F_s can be obtained as:

$$dF_s = dF - dF_f - dF_{surf} \tag{A11}$$

Substitution of equations (A2-A3) and (A6-A10) into equation (A11) produces the energy balance as:

$$dF_s = \sigma_{ij} d\varepsilon_{ij} + p_f^s d\varepsilon_v + (p_m - p_m^s) dn_m + \left(p_f - p_f^s\right) dn_f \tag{A12}$$

where $p_f^s = \xi_f \sigma^s$; $p_m^s = \xi_m \sigma^s$; $\xi_f = \frac{\partial A_p}{\partial(n_f - \varepsilon_v)}$; $\xi_m = \frac{\partial A_p}{\partial n_m}$.

Replacing the volumetric strain with ε_{ii}, equation (A12) can be rearranged as:

$$dF_s = \sigma_{ij}^a d\varepsilon_{ij} + p_m^a dn_m + p_f^a dn_f \tag{A13}$$

where $\sigma_{ij}^a = \sigma_{ij} + p_f^s \delta_{ij}$; $p_m^a = p_m - p_m^s$; $p_f^a = p_f - p_f^s$, and $\delta_{ii} = 1$, $\delta_{ij} = 0$.

It can be seen from equation (A13) that when gas adsorption is involved, the role of surface stress can be described macroscopically via p_m^s and p_f^s, the fluid pressures p_m, p_f are modified as p_m^a, p_f^a.

Introducing energy G_s instead of the solid free energy, F_s is more convenient to consider the opposite of partial Legendre transform of solid free energy with regards to n_m and n_f:[31]

$$G_s = F_s - p_m^a n_m - p_f^a n_f \tag{A14}$$

Substation of equation (A14) into (A13) yields:

$$dG_s = \sigma_{ij}^a d\varepsilon_{ij} - n_m dp_m^a - n_f dp_f^a \tag{A15}$$

From equation (A15), the state equation of dual poro-elasticity can be written in the form:

$$G_s = G_s\left(\varepsilon_{ij}, p_m^a, p_f^a\right) \tag{A16}$$

$$\sigma_{ij}^a = \frac{\partial G_s}{\partial \varepsilon_{ij}}; \quad n_m = \frac{\partial G_s}{\partial p_m^a}; \quad n_f = \frac{\partial G_s}{\partial p_f^a} \tag{A17}$$

Differentiating state equation (A17) and considering the Maxwell's symmetry relations:

$$\frac{\partial \sigma_{ij}^a}{\partial \varepsilon_{kl}} = \frac{\partial \sigma_{kl}^a}{\partial \varepsilon_{ij}}; \quad \frac{\partial \sigma_{ij}^a}{\partial p_m^a} = -\frac{\partial n_m}{\partial \varepsilon_{ij}}; \quad \frac{\partial \sigma_{ij}^a}{\partial p_f^a} = -\frac{\partial n_f}{\partial \varepsilon_{ij}} \tag{A18}$$

lead to

$$d\sigma_{ij}^a + b_{mij} dp_m^a + b_{fij} dp_f^a = C_{ijkl} d\varepsilon_{kl} \tag{A19}$$

where $C_{ijkl} = \frac{\partial^2 G_s}{\partial \varepsilon_{ij} \varepsilon_{kl}}$ and $b_{mij} = -\frac{\partial^2 G_s}{\partial \varepsilon_{ij} \partial p_m^a}$. is the ijth component of Biot's effective stress coefficient tensor for pore fluid pressure with symmetry $b_{mij} = b_{mji}$ due to stress and strain symmetry. From equation (A18), b_{mij} linearly relates the stress increment to the pore fluid pressure increment in an evolution when fluid pressure in fractures and strain is held constant, i.e. $d\varepsilon_{ij} = 0$. $b_{fij} = -\frac{\partial^2 G_s}{\partial \varepsilon_{ij} \partial p_f^a}$ is the ijth component of Biot's effective stress coefficient tensor for fracture fluid pressure with symmetry $b_{fij} = b_{fji}$, from equation (A18), b_{fij} linearly relates the stress increment to the fracture fluid pressure increment in an evolution when strain is held constant. It is worth pointing out that the effective stress coefficients b_{mij}, b_{fij} are a second rank tensor, suggesting that pore pressure modifies not only effective normal stresses, but also effective shear stresses. However, the latter effect is vanished under the isotropic condition.

Based on the effective stress concept, equation (A19) can be rewritten as:

$$d\sigma_{eij}^{'} = C_{ijkl} d\varepsilon_{kl} \tag{A20}$$

where

$$d\sigma_{eij}^{'} = d\sigma_{ij}^a + b_{mij} dp_m^a + b_{fij} dp_f^a \tag{A21}$$

may be regarded as the effective stress for fractured porous media saturated with adsorptive fluids.

Replacing the counterpart terms in effective stress $\sigma_{eij}^{'}$ and integrating with assumption of zero initial stress and fluid pressure give:

$$\sigma_{eij}^{'} = \sigma_{ij} + p_f^s \delta_{ij} + b_{mij}\left(p_m - p_m^s\right) + b_{fij}\left(p_f - p_f^s\right) \tag{A22}$$

If no adsorption occurs on the interface between a solid and a fluid, equation (A22) can be reduced as:

$$\sigma_{eij}^{'} = \sigma_{ij} + b_{mij} p_m + b_{fij} p_f \tag{A23}$$

Compared to conventional constitutive equations of effective stress for anisotropic dual poro-elasticity, equation (A22) shows that in order to prevent any deformation and porosity changes with respect to the reference configuration, a pre-stress p_f^s, an initial pressure in pores p_m^s and in fractures p_f^s have to be applied against the effects induced by the surface stress change resulting from gas adsorption.

Nomenclatures

A	Area of fractures per unit volume of the rock
a	Fracture aperture
A_p	Surface area of the pores
b_{fij}	Effective stress coefficients for fluid pressure in fractures
b_L	Langmuir pressure constant
b_{mij}	Effective stress coefficients for fluid pressure in matrices
C_{fij}	Directional fracture compressibility
C_{ijkl}	Elastic stiffness tensor
d	Compliance coefficient
D_{ijkl}	Elastic compliance tensor
D_f	Fracture intensity
E_i	Young's modulus in the ith direction
f_{ai}	Sorption induced change of compressibility in the ith direction
F	Helmholtz free energy of system per unit volume
F_s	Helmholtz free energy stored in solid skeleton
F_f	Helmholtz free energy stored in the fluid
F_{surf}	Helmholtz free energy stored on pore surface
i, j, k, l	Index
k	Fracture permeability

k_i	Fracture permeability in the ith direction
k_{i0}	Fracture permeability in the ith direction at the reference stress state
n_f	Fracture porosity
n_{fi}	Fracture porosity in i direction
n_g	Number of gas components in the mixture
n_m	Coal matrix porosity
p	Fluid pressure at equilibrium state
p_f	Fluid pressure in fracturs
p_f^s	Adsorption induced stress in fractures
p_m	Fluid pressure in matrix pores
p_m^s	Adsorption induced stress in matrix
R	Universal gas constant
R_c	Fracture connectivity
T	Temperature
$\overline{V}_b$	Molar volume
x_m	Molar fraction of the mth gas component
α_{ij}	Fracture compressibility change rate
γ_{mi}	Weakening coefficient of mth gas component
σ_{ij}	Components of total stress
σ^s	Surface stress
σ'_{eij}	Effective stress for bulk coal
σ'_{ii}	Effective stress only acting on coal fractures in ith direction
σ'_{ii0}	Effective stress only acting on coal fractures at the reference stress state
ε_{ij}	Component of second-order strain tensor
ε_v	volumetric stain of bulk coal
ε_{vm}	Volumetric strain of coal matrix
ν_{ij}	Poisson's ratio
Γ	Number of moles of fluid molecules adsorbed
Γ^{max}	adsorption capacity of fluid per unit adsorption surface
μ_m	Molar chemical potentials of the fluid in matrix pores
μ_f	Molar chemical potentials of the fluid in fractures
ρ_m	Molar density of the fluid in matrix pores
ρ_f	Molar density of the fluid in fractures
ρ_m^b	Molar density of bulk phase in matrix pores
ρ_m^a	Molar density of adsorbed phase in matrix pores
δ_{ij}	Kronecker delta

References

1 Godec ML, Jonsson H, Basava-Reddi L. Potential global implications of gas production from shales and coal for geological CO2 storage. *Energy Proc*. 2013;37:6656–6666.
2 Pan Z, Ye J, Zhou F, Tan Y, Connell LD, Fan J. CO_2 storage in coal to enhance coalbed methane recovery: a review of field experiments in China. *Int Geol Rev*. 2018;60(5-6):754–776.
3 Chen M. *Modelling of Gas Transport in Coal-A Hybrid Coupled Dual Porosity and Discrete Fracture Approach*. 2019.
4 Fujioka M, Yamaguchi S, Nako M. CO_2-ECBM field tests in the Ishikari coal basin of Japan. *Int J Coal Geol.* 2010;82(3-4):287–298.
5 van Bergen F, Pagnier H, Krzystolik P. Field experiment of enhanced coalbed methane-CO_2 in the upper Silesian basin of Poland. *Environ Geosci.* 2006;13(3):201–224.
6 Connell L, Pan Z, Camilleri M, et al. Description of a CO2 enhanced coal bed methane field trial using a multi-lateral horizontal well. *Int J Greenh Gas Control*. 2014;26:204–219.
7 Chen M, Hosking LJ, Sandford RJ, Thomas HR. Numerical analysis of improvements to CO_2 injectivity in coal seams through stimulated fracture connection to the injection well. *Rock Mech Rock Eng*. 2020:1–20.
8 Chen M, Hosking LJ, Sandford RJ, Thomas HR. Dual porosity modelling of the coupled mechanical response of coal to gas flow and adsorption. *Int J Coal Geol.* 2019;205:115–125.
9 Pan Z, Connell LD. Modelling permeability for coal reservoirs: a review of analytical models and testing data. *Int J Coal Geol*. 2012;92:1–44.
10 Harpalani S, Chen G. Influence of gas production induced volumetric strain on permeability of coal. *Geotech Geol Eng*. 1997;15(4):303–325.
11 Laubach S, Marrett R, Olson J, Scott A. Characteristics and origins of coal cleat: a review. *Int J Coal Geol*. 1998;35(1):175–207.
12 Seidle J. *Fundamentals of Coalbed Methane Reservoir Engineering*. PennWell Books; 2011.
13 Koenig R, Stubbs P. Interference testing of a coalbed methane reservoir. In: *SPE Unconventional Gas Technology Symposium*. Society of Petroleum Engineers; 1986.
14 Massarotto P, Rudolph V, Golding S. *Anistropic Permeability Characterisation of Permian Coals*. 2003.
15 Day S, Fry R, Sakurovs R. Swelling of Australian coals in supercritical CO_2. *Int J Coal Geol.* 2008;74(1):41–52.
16 Pan Z, Connell LD. Modelling of anisotropic coal swelling and its impact on permeability behaviour for primary and enhanced coalbed methane recovery. *Int J Coal Geol.* 2011;85(3-4):257–267.
17 Liu Y, Yin G, Li M, et al. Anisotropic mechanical properties and the permeability evolution of cubic coal under true triaxial stress paths. *Rock Mech Rock Eng*. 2019;52(8):2505–2521.
18 Liu J, Chen Z, Elsworth D, Qu H, Chen D. Interactions of multiple processes during CBM extraction: a critical review. *Int J Coal Geol*. 2011;87(3-4):175–189.
19 Gu F, Chalaturnyk R. Permeability and porosity models considering anisotropy and discontinuity of coalbeds and application in coupled simulation. *J Petrol Sci Eng*. 2010;74(3-4):113–131.
20 Liu S, Wang Y, Harpalani S. Anisotropy characteristics of coal shrinkage/swelling and its impact on coal permeability evolution with CO_2 injection. *Greenhouse Gases: Sci Technol.* 2016;6(5):615–632.
21 Wang G, Massarotto P, Rudolph V. An improved permeability model of coal for coalbed methane recovery and CO_2 geosequestration. *Int J Coal Geol*. 2009;77(1-2):127–136.
22 Liu J, Chen Z, Elsworth D, Miao X, Mao X. Linking gas-sorption induced changes in coal permeability to directional strains through a modulus reduction ratio. *Int J Coal Geol.* 2010;83(1):21–30.
23 Pan Z, Connell LD. A theoretical model for gas adsorption-induced coal swelling. *Int J Coal Geol.* 2007;69(4):243–252.
24 Gu F, Chalaturnyk R. Numerical simulation of stress and strain due to gas sorption/desorption and their effects on in situ permeability of coalbeds. *J Can Petrol Technol.* 2006;45(10).
25 Liu H-H, Rutqvist J, Berryman JG. On the relationship between stress and elastic strain for porous and fractured rock. *Int J Rock Mech Min Sci.* 2009;46(2):289–296.

26 Peng S, Fang Z, Shen J, Xu J, Wang G. Effects of gas sorption-induced swelling/shrinkage on the cleat compressibility of coal under different bedding directions. *Sci Rep*. 2017;7(1):1–10.
27 Jaeger JC, Cook NG, Zimmerman R. *Fundamentals of Rock Mechanics*. John Wiley & Sons; 2009.
28 Nikoosokhan S, Brochard L, Vandamme M, et al. CO_2 storage in coal seams: coupling surface adsorption and strain. *Geomech CO Storag Facilities*. 2012:115–132.
29 Zhang Y. Mechanics of adsorption–deformation coupling in porous media. *J Mech Phys Solid*. 2018;114:31–54.
30 Szwilski A. Determination of the anisotropic elastic moduli of coal. *Int J Rock Mech Min Sci Geomech Abstracts*. 1984;21:3–12. Elsevier.
31 Coussy O. *Poromechanics*. John Wiley & Sons; 2004.
32 Witherspoon PA, Wang JS, Iwai K, Gale JE. Validity of cubic law for fluid flow in a deformable rock fracture. *Water Resour Res*. 1980;16(6):1016–1024.
33 Chen D, Pan Z, Ye Z. Dependence of gas shale fracture permeability on effective stress and reservoir pressure: model match and insights. *Fuel*. 2015;139:383–392.
34 Liu H-H, Wei M-Y, Rutqvist J. Normal-stress dependence of fracture hydraulic properties including two-phase flow properties. *Hydrogeol J*. 2013;21(2):371–382.
35 Duan M, Jiang C, Gan Q, Zhao H, Yang Y, Li Z. Study on permeability anisotropy of bedded coal under true triaxial stress and its application. *Transport Porous Media*. 2020;131(3):1007–1035.
36 Lu J, Yin G, Deng B, et al. Permeability characteristics of layered composite coal-rock under true triaxial stress conditions. *J Nat Gas Sci Eng*. 2019;66:60–76.
37 Pan Z, Connell LD, Camilleri M. Laboratory characterisation of coal reservoir permeability for primary and enhanced coalbed methane recovery. *Int J Coal Geol*. 2010;82(3-4):252–261.
38 McKee CR, Bumb AC, Koenig RA. Stress-dependent permeability and porosity of coal and other geologic formations. *SPE Form Eval*. 1988;3:81–91, 01.
39 Masoudian MS, Airey DW, El-Zein A. Experimental investigations on the effect of CO_2 on mechanics of coal. *Int J Coal Geol*. 2014;128:12–23.
40 Zagorščak R, Thomas HR. Effects of subcritical and supercritical CO_2 sorption on deformation and failure of high-rank coals. *Int J Coal Geol*. 2018;199:113–123.
41 Sampath K, Perera M, Ranjith P, Matthai S. CO_2 interaction induced mechanical characteristics alterations in coal: a review. *Int J Coal Geol*. 2019;204:113–129.
42 Seidle J, Jeansonne M, Erickson D. *Application of Matchstick Geometry to Stress Dependent Permeability in Coals. SPE Rocky Mountain Regional Meeting*. Society of Petroleum Engineers; 1992.
43 Cui X, Bustin RM. Volumetric strain associated with methane desorption and its impact on coalbed gas production from deep coal seams. *AAPG Bull*. 2005;89(9):1181–1202.
44 Shi J, Durucan S. Drawdown induced changes in permeability of coalbeds: a new interpretation of the reservoir response to primary recovery. *Transport Porous Media*. 2004;56(1):1–16.
45 Robertson EP. *Measurement and Modeling of Sorption-Induced Strain and Permeability Changes in Coal*. Idaho National Laboratory (INL); 2005.
46 Hol S, Peach CJ, Spiers CJ. Effect of 3-D stress state on adsorption of CO_2 by coal. *Int J Coal Geol*. 2012;93:1–15.
47 Pini R, Ottiger S, Burlini L, Storti G, Mazzotti M. Role of adsorption and swelling on the dynamics of gas injection in coal. *J Geophys Res Solid Earth*. 2009;114(B4).
48 Lin W, Tang G-Q, Kovscek AR. Sorption-induced permeability change of coal during gas-injection processes. *SPE Reservoir Eval Eng*. 2008;11:792–802, 04.
49 Chen Z, Pan Z, Liu J, Connell LD, Elsworth D. Effect of the effective stress coefficient and sorption-induced strain on the evolution of coal permeability: experimental observations. *Int J Greenh Gas Control*. 2011;5(5):1284–1293.
50 Li J, Liu D, Lu S, Yao Y, Xue H. Evaluation and modeling of the CO2 permeability variation by coupling effective pore size evolution in anthracite coal. *Energy Fuels*. 2015;29(2):717–723.
51 Lin W, Kovscek AR. Gas sorption and the consequent volumetric and permeability change of coal I: experimental. *Transport Porous Media*. 2014;105(2):371–389.
52 Mitra A, Harpalani S, Liu S. Laboratory measurement and modeling of coal permeability with continued methane production: Part 1–Laboratory results. *Fuel*. 2012;94:110–116.
53 Seomoon H, Lee M, Sung W. Analysis of sorption-induced permeability reduction considering gas diffusion phenomenon in coal seam reservoir. *Transport Porous Media*. 2015;108(3):713–729.
54 Ma Q, Harpalani S, Liu S. A simplified permeability model for coalbed methane reservoirs based on matchstick strain and constant volume theory. *Int J Coal Geol*. 2011;85(1):43–48.
55 Meng Y, Li Z. Triaxial experiments on adsorption deformation and permeability of different sorbing gases in anthracite coal. *J Nat Gas Sci Eng*. 2017;46:59–70.
56 Palmer I, Mansoori J. *How Permeability Depends on Stress and Pore Pressure in Coalbeds: A New Model. SPE Annual Technical Conference and Exhibition*. Society of Petroleum Engineers; 1996.
57 Anggara F, Sasaki K, Sugai Y. The correlation between coal swelling and permeability during CO_2 sequestration: a case study using Kushiro low rank coals. *Int J Coal Geol*. 2016;166:62–70.
58 Kumar H, Elsworth D, Liu J, Pone D, Mathews JP. Permeability evolution of propped artificial fractures in coal on injection of CO_2. *J Petrol Sci Eng*. 2015;133:695–704.
59 Li Y, Wang Y, Wang J, Pan Z. Variation in permeability during CO_2–CH4 displacement in coal seams: Part 1–Experimental insights. *Fuel*. 2020;263:116666.
60 Niu Q, Cao L, Sang S, Zhou X, Wang Z, Wu Z. The adsorption-swelling and permeability characteristics of natural and reconstituted anthracite coals. *Energy*. 2017;141:2206–2217.
61 Coussy O. *Mechanics and Physics of Porous Solids*. John Wiley & Sons; 2011.
62 Vandamme M, Brochard L, Lecampion B, Coussy O. Adsorption and strain: the CO_2-induced swelling of coal. *J Mech Phys Solid*. 2010;58(10):1489–1505.